Precise construction of PCBM aggregates for polymer solar cells *via* multi-step controlled solvent vapor annealing†

Haowei Tang,[ab] Guanghao Lu,[ab] Ligui Li,[ab] Jun Li,[ab] Yuzhen Wang[ab] and Xiaoniu Yang*[a]

Received 25th August 2009, Accepted 22nd October 2009
First published as an Advance Article on the web 25th November 2009
DOI: 10.1039/b917533d

Polymer solar cells based on poly(3-hexylthiophene)/[6,6]-phenyl-C_{61}-butyric-acid methyl ester (P3HT/PCBM) composite are one of state-of-the-art polymer photovoltaic devices in terms of performance. In this work, we applied two-step controlled solvent vapor annealing (C-SVA) to achieve an optimized morphology for the photoactive layer with both an appropriate size of PCBM aggregates and an improved crystallinity of P3HT. As revealed by bright-field transmission electron microscopy (TEM), and atomic force microscopy (AFM), X-ray diffraction (XRD) and UV-Vis spectroscopy, PCBM forms aggregates with sizes of *ca.* 30 nm during the first step C-SVA in tetrahydrofuran vapor. The second step treatment using carbon disulfide vapor on one hand reduces the large size of these PCBM aggregates to *ca.* 20 nm, and on the other hand substantially increases the crystallinity of P3HT. The polymer solar cells employing a thus-treated composite film gave a power conversion efficiency as high as 3.9%, in contrast to 3.2% for the thermally annealed device under the same characterization conditions. This result shows the importance of a precisely controlled morphology of the photoactive layer in device performance.

Introduction

Polymer solar cells are attracting more and more attention due to their distinct advantages, such as low production cost, mechanical flexibility and ease of achieving a large-area device by production line, as compared with traditional inorganic photovoltaic devices.[1–4] Polymer solar cells with a power conversion efficiency (PCE) of more than 5% have been currently achieved, which are very promising candidates for a clean and renewable energy source.[5–7] However, the performance of polymer solar cells is heavily dependent on the morphology of components involved in photoactive layers.[8–11] Due to the inherent limited exciton diffusion length in organic semiconductors, the phase separation scale between the donor and acceptor materials should be on the nano-scale to ensure highly efficient exciton dissociation.[12–15] The introduction of the bulk-heterojunction concept to polymer solar cells, in which electron donor and acceptor materials are homogeneously mixed together to form a photoactive layer, has been a milestone in this research field.[16] On the other hand, continuous pathways through the photoactive layers are required for direct and faster free charge carrier transport to the corresponding electrodes, which implies that increased phase separation but still on the nano-scale is necessary.[17–20] Spin coating is one of the most frequently used techniques to prepare large-area thin film electronic devices based on polymers.[21] However, due to the fast solvent evaporation, the crystallization or aggregation of the components involved will be kinetically suppressed, forming an extremely homogeneous film.[22] To remedy this drawback, pre- or post- treatments such as choice of solvent,[23–26] thermal annealing[27–29] and solvent vapor annealing[30,31] have been usually adopted to construct interpenetrating networks. However, at elevated temperature the conjugated polymers will suffer from the risk of degradation. Additionally, great care is needed to prevent large-scale phase separation.[32] Controlled solvent vapor annealing (C-SVA) has thus been proposed and employed to construct a precise morphology for the substantially improved device performance of polymer solar cells based on P3AT/C60 composites.[30] Actually, the powerful morphology construction of the C-SVA approach has already been demonstrated.[33–35] However, in the application of C-SVA to the multicomponent system, especially for those systems for which the components involved have quite different interactions with a solvent vapor, it is difficult to achieve precisely the desired morphology for each component using a single-step C-SVA. Therefore, a multi-step C-SVA method is required so as to construct a precise morphology for the whole film. Thus, a large variety of solvents are available for the choices, which endow multi-step methods with even higher potential.

As one of the successful polymer photovoltaic devices with high performance, and a model bulk-heterojunction for charge separation and transport, poly(3-hexylthiophene)/[6,6]-phenyl-C_{61}-butyric-acid methyl ester (P3HT/PCBM) based solar cells have been intensively studied. Although currently the performance of polymer solar cells has been enhanced by many pre- or post- treatments, in fact most of these methods are mainly aimed at improving the crystallinity of P3HT for effective hole transport rather than the morphological optimization of the PCBM

[a]*State Key Laboratory of Polymer Physics and Chemistry, Changchun Institute of Applied Chemistry, Chinese Academy of Sciences, Renmin Str. 5625, Changchun, 130022, P. R. China. E-mail: xnyang@ciac.jl.cn*
[b]*Graduate School of the Chinese Academy of Sciences, Beijing, 100049, P. R. China*

† Electronic supplementary information (ESI) available: UV/Vis absorption spectra; TEM images; *J–V* curves. See DOI: 10.1039/b917533d

phase. Herein we demonstrate the application of a two-step C-SVA in tuning the nano-scale phase separation, especially the morphological structure of PCBM component, for poly-(3-hexylthiophene)/[6,6]-phenyl-C_{61}-butyric-acid methyl ester (P3HT/PCBM) composite film towards high performance photovoltaic devices.

Experimental

Materials

Poly(3-hexylthiophene) (P3HT) (M_w = 56 000 g mol^{-1}, regioregularity > 98.5%, polydispersity index PDI = 2.23) was purchased from Rieke Metals Inc. PCBM and *o*-dichlorobenzene (ODCB, anhydrous, 99%) were purchased from Sigma-Aldrich. Carbon disulfide (CS_2) and tetrahydrofuran (THF) were purchased from Sinopharm Chemical Reagent Co.

Sample preparations

P3HT-PCBM (1 : 1, w/w) was dissolved in ODCB to achieve solution with P3HT concentration 10 mg mL^{-1}. Thin films of thicknesses *ca.* 100 nm for atomic force microscopy (AFM), UV/Vis, transmission electron microscopy (TEM), wide-angle X-ray diffraction (WXRD) and device fabrication were prepared by spin-coating (Laurell Spin Processor WS-400B 6 NPP Lite) on the precleaned substrates.

The indium tin oxide (ITO)-coated glass substrate for polymer solar cells was cleaned in detergent, deionized water, isopropyl alcohol and acetone by ultrasonic treatment. After treating the substrate with UV ozone for 20 min, poly(3,4-ethylenedioxythiophene):poly(styrenesulfonate) (PEDOT:PSS) (Baytron P) was spin-coated on this well-cleaned ITO. The photoactive layer was prepared by spin-coating blend solution on the above substrate under ambient atmosphere. Finally the devices were completed by evaporation of a 1 nm LiF layer and subsequently a 100 nm Al as the cathode.

The C-SVA environment was created by pouring 20 mL solvent into a long glass tube (6 cm in diameter and 120 cm in length). Solvent vapor at the bottom can diffuse along the tube to the top which exposed to ambient atmosphere. Stable vapor gradient along the tube could be obtained after 10–15 h when liquid solvent was placed at the bottom. Gas chromatography was employed to determine the vapor pressures associated with the different positions along the tube. In different C-SVA the required solvent vapor pressure can be precisely chosen upon rapidly placing the composite film at the given position in the tube.

Characterization

TEM was performed on a JEOL JEM-1011 transmission electron microscope operated at an acceleration voltage of 100 kV. First, thin films were floated on water and then transferred onto a copper grid. All the samples for TEM experiment were dried at room temperature for more than 12 h, and all the SAED patterns were performed using a fixed magnification and the same current density and exposure time for SAED acquisition.

UV/Vis measurements were carried out using a Perkin–Elmer UV/Vis Lambda 750 spectrometer with 2.0-nm slit width.

WXRD profiles were obtained by using a Bruker D8 Discover Reflector with an X-ray generation power of 40 kV tube voltage and 40 mA tube current. The diffraction was recorded at a θ–2θ symmetry scanning mode with a scan angle 2θ from 3° to 25°.

AFM measurements were performed on an Agilent 5500 in tapping mode in the ambient atmosphere.

To ensure stable spectrum and intensity throughout the device characterization, all the photovoltaic cells were measured under illumination by a tungsten–halogen lamp (filtered by a Schott KG1 and GG385 filter) at an intensity of 100 mW cm^{-2}. The *J*–*V* characteristics were recorded in a glove box using a Keithley 2400 source meter.

Results and discussion

The P3HT/PCBM composite is so far still one of the most successful systems for polymer solar cells in terms of the power conversion efficiency.[27,36] As crystallizable materials, the crystallinity of both P3HT and PCBM components could be enhanced upon exposure to the solvent vapor.[37–40] Therefore, in this work C-SVA using carbon bisulfide (CS_2) and tetrahydrofuran (THF) vapor, respectively, were employed to manipulate the morphology of P3HT/PCBM composite towards improved performance of the corresponding photovoltaic devices. Herein, we apply the combination (*p*, *t*) to describe the two important parameters in C-SVA, where *p* is the relative vapor pressure and *t* is the annealing time at a given vapor pressure, respectively. After deliberately choosing the parameters for C-SVA treatment, *e.g.* vapor pressure, the device performance could be certainly improved upon the treatment using either solvent (Fig. 1). However, the performance of the thus treated solar cells is still not able to compete with those devices upon post-thermal annealing. Typically, the parameter fill factor (FF) of the device upon THF annealing could be substantially improved to higher than 0.6. However, the short circuit current (J_{sc}) is only slightly increased to 6 mA cm^{-2}. With further increased vapor pressure of THF, the power conversion efficiency (PCE) of the device, however, would heavily drop down. For instances, the PCE of the device upon THF treatment at (0.92, 5 s) is comparable to that of the pristine cells of 1.21%; if a saturated THF vapor is used during the treatment, the typical parameters of the device, *e.g.* J_{sc} and FF decrease to 4.36 mA cm^{-2} and 0.35, respectively, produce a rather low PCE of 0.65%. However, if CS_2 is employed as the medium for solvent vapor treatment, J_{sc} could be increased to higher than 7 mA cm^{-2}, but FF does not get obvious improvement. The UV-Vis spectra of the composite films upon C-SVA treatments using THF show that the absorption at 607 nm, which is attributed to the π–π packing/crystallization of P3HT chains, has a comparable intensity with that of the pristine film. However, for those films undergoing CS_2 treatment this absorption is somewhat enhanced, in particular at high vapor pressure (Fig. S1 in the ESI†).[41] During C-SVA, solvent molecules were absorbed by the polymer film. It has been shown that THF molecules could substantially increase the mobility of PCBM molecules within P3HT/PCBM composite film, which would lead to formation of PCBM aggregates (Fig. S2†). Therefore, with increased solvent vapor pressure the treatment time should be correspondingly reduced so as to prevent large-scale phase separation. However, for regioregular P3HT, THF is

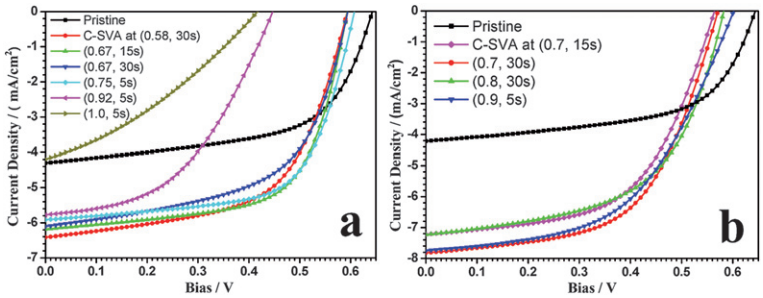

Fig. 1 *J-V* characteristics of the P3HT/PCBM (1 : 1 in wt) devices prepared upon single-step C-SVA treatment using (a) THF vapor and (b) CS_2 vapor.

not a good solvent, so the limited amount of THF absorbed cannot endow the P3HT chain with enough mobility to effectively crystallize. In contrast, CS_2 is a good solvent for both P3HT and PCBM, so CS_2 vapor is able to substantially improve P3HT crystallinity in the composite film. On the other hand, during C-SVA PCBM was fully dissolved within P3HT/CS_2 film so no obvious change of the PCBM component occurred. As a consequence, the morphology of the photoactive layer based on the P3HT/PCBM composite could only be partially optimized upon C-SVA using a single solvent vapor. A multi-step C-SVA approach was thus introduced in this work so as to comprehensively utilize the advantage of each vapor to eventually achieve a highly optimized morphology for P3HT/PCBM composite with both substantially increased crystallinity of P3HT and enhanced but still controllable nanoscale PCBM aggregates. Fig. 2 schematically gives a two-step C-SVA treatment by successively using THF and CS_2 vapor.

As shown by the bright-field transmission electron microscopy (BF-TEM) image (Fig. 3a), upon C-SVA treatment at (1.0, 5 s) using THF vapor, the morphological features of the film obviously increase, as a consequence of homogeneously emerging dark domains which are ascribed to PCBM aggregates. The AFM topography image (Fig. 3b) also confirms these PCBM-rich domains as remarkable granular clusters, which have statistically average diameters of 29 nm for the top and 23 nm for the bottom side (Fig. 3c), respectively. A smaller cluster size at the bottom might be attributed to the decreased mobility of PCBM molecules resulting from spatial confinement by the substrate. From the selected-area electron diffraction (SAED) pattern we can only observe a diffuse halo contributed by PCBM, indicating these PCBM-rich domains are composed of randomly distributed PCBM nanocrystals.[42] However, if the annealing time is extended to 30 s large PCBM single crystals with a hexagonal shape appear (Fig. S3†). Afterwards, this THF vapor treated film at (1.0, 5 s) is subsequently placed in an environment filled with CS_2 vapor to perform the second step of C-SVA. Upon CS_2 vapor treatment at (0.8, 15 s), as revealed by AFM images, the size of those PCBM-rich clusters is reduced to a statistical diameter of 19 nm (top) (Fig. 2e) and 12 nm (bottom) (Fig. 2f), respectively, which have already clearly implied that the PCBM-rich clusters previously formed during THF vapor treatment were partially dissolved during the subsequent CS_2 vapor annealing.

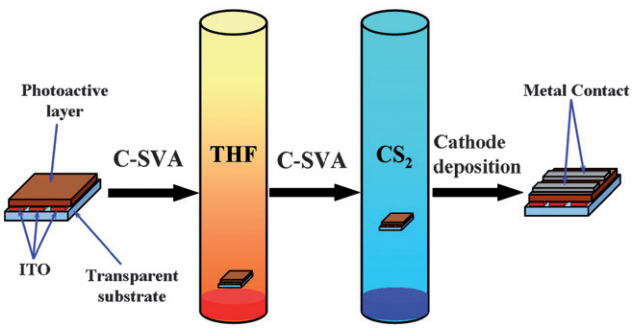

Fig. 2 Scheme of the fabrication of P3HT/PCBM solar cells using two-step C-SVA approach.

The size evolution of PCBM clusters during the two-step C-SVA can be further revealed by the changes in UV-Vis absorption spectra. In Fig. 4a, all the curves show four peaks, the peak centered at around 334 nm is a typical absorption of PCBM and the position of this peak will change slightly if the dimension of PCBM domains varies.[43] For the film with larger PCBM-rich domains as obtained upon THF vapor treatment, this peak undergoes a red-shift from 333.9 nm in a pristine film to 335.8 nm. While exposed to CS_2 vapor, it will blue-shift back to 334.4 nm, indicating that smaller PCBM clusters are constructed in this composite, which is consistent with the morphological observations (TEM and AFM). On the other hand, after two-step C-SVA, the main absorbance at 517 nm of P3HT in the composite film increases and the other two bands at 560 nm and 607 nm become more prominent as compared with those in the pristine films.[44] Moreover, as shown in WXRD experimental results (Fig. 5), the intensity of main peak around $2\theta = 5.4°$, which belongs to the crystallographic (100) plane of RR-P3HT does not substantially increase upon the first step C-SVA in THF vapor (1.0, 5 s). However, after the second step C-SVA in CS_2 vapor (0.8, 15 s), the intensity of this characteristic peak becomes much stronger. These results confirmed above conclusion that in our experimental conditions, CS_2 instead of THF is mainly responsible for the enhanced crystallinity of P3HT in the composite film.

The feasibility of using this two-step C-SVA method to construct an optimized morphology for photovoltaic devices has been proven by the improvement of the thus-obtained device performance. As is shown in Fig. 4b, for the device based on a pristine P3HT/PCBM film, although a relatively high V_{oc} of 0.66 V is achieved, the low J_{sc} and FF of 5.02 mA cm^{-2} and 48%, respectively, contribute to a PCE of only 1.60%. Similar to typical post-thermal treatment, although a somewhat decreased V_{oc} of 0.58 V is obtained upon thermal annealing, the substantial

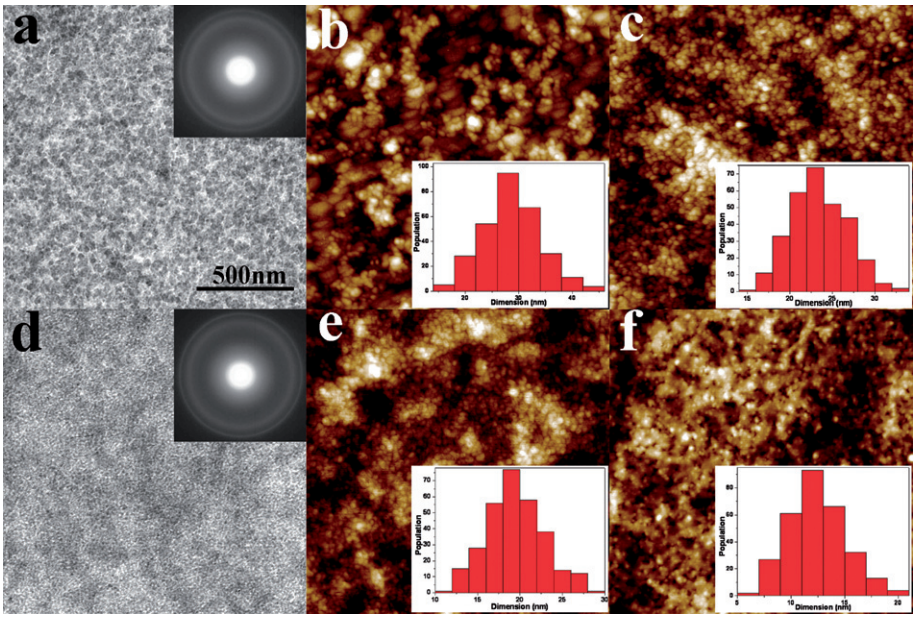

Fig. 3 BF-TEM images and corresponding SAED patterns of P3HT/PCBM composite films spin-coated from ODCB. (a) Single-step in THF at (1.0, 5 s); (d) Two-step in THF at (1.0, 5 s) and then in CS_2 at (0.8, 15 s). AFM topography images of composite film and corresponding size distribution of PCBM clusters. (b,c) Single-step; (e, f) two-step. (b,e) Top-side; (c,f) bottom-side.

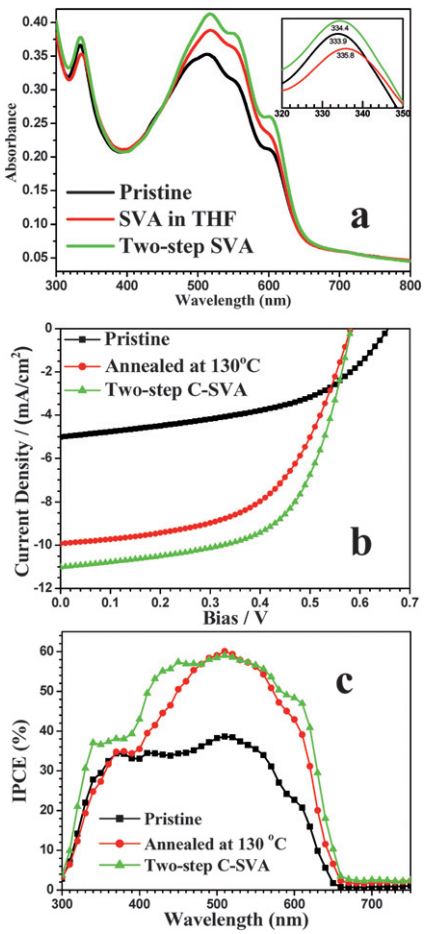

Fig. 4 UV-Vis absorption spectra (a), *J*–*V* characteristics (b) and IPCE (c) of P3HT/PCBM composite film or corresponding PV device prepared upon different treatments.

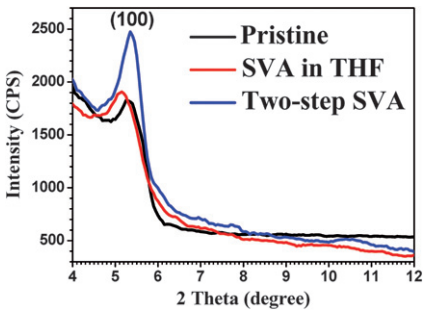

Fig. 5 WAXD profiles of P3HT/PCBM composite films upon different C-SVA treatments.

increase of J_{sc} and FF eventually contribute to an improved PCE of 3.20% (Fig. 4b). However, more promising device performance is achieved by using the two-step C-SVA. As is summarized in Table 1, the device subjected to two-step C-SVA shows $V_{oc} = 0.58$V, $J_{sc} = 11.01$ mA cm^{-2}, FF = 61%, and PCE = 3.87%, which is more than 20% higher than that obtained *via* the thermal annealing method. The enhancement of device efficiency could be verified by monochromatic incident photon-to-electron conversion efficiency (IPCE) measurement. In Fig. 4c, the IPCE value is below 40% within the whole wavelength range for

Table 1 Comparison of deviceperformance of P3HT/PCBM (1 : 1 by wt) polymer solar cells upon various treatments

	V_{oc}	J_{sc}	FF	PCE
Pristine	0.66	5.02	0.48	1.6
Two-step C-SVA	0.58	11.01	0.61	3.9
Thermal annealing	0.58	9.92	0.55	3.2

pristine device. Upon thermal annealing, IPCE is increased overall for the spectra range measured, showing a maximum around 60% at 510 nm, and becomes broader resulting from red-shift of the spectra. In contrast, for the device after two-step C-SVA treatment, the range of response spectra with IPCE value beyond 50% becomes broader from 410 nm to 590 nm (Fig. 4c). Particularly, the IPCE value is still higher than 45% at 610 nm. These results give strong evidence that the enhanced optical absorption and optimized morphology has already been constructed in the photovoltaic layer after two-step C-SVA.

In comparison to the morphological result obtained from the two-step C-SVA, for the film upon first step C-SVA treatment in THF vapor at (1.0, 5 s), the PCBM clusters are relative large in the composite, which reduces the interface area for exciton dissociation and results in the low device performance (Fig. 1a). In the second step treatment CS_2 vapor not only enhances the crystallinity of P3HT but also partially dissolves those PCBM aggregates, which brings the composite film to an optimized morphology. Upon this two-step C-SVA treatment, the PCBM domains have been reduced to some extent, but they can still form continuous pathways for fast charge transport while maintaining enough interface area for efficient exciton dissociation, which will contribute to improved photovoltaic performance. We speculate that the final morphology of the composite is the most important factor to dominate the ultimate device performance. To prove it we prepared more devices subjected to this two-step C-SVA treatment with various parameters. By controlling mainly the treatment time and solvent vapor pressure, the morphology of the photoactive layer and corresponding device performance could be further tuned. For instance, if the device is treated in THF vapor at (1.0, 15 s) and then annealed in CS_2 at (0.8, 15 s), a PCE of 3.51% could be achieved. However, if the treatment time in CS_2 is prolonged to 30 s at (0.8, 30s) but the same parameters for the first step treatment in THF vapor at (1.0, 5 s) is used, a decreased PCE of 3.15% is obtained (Fig. S5†). In the corresponding TEM images PCBM-rich domains could be clearly identified, which contribute to remarkably enhanced device performance (Fig. S4†). Alternatively, the treatment in THF vapor is fixed at (1.0, 5 s), but the second step treatment in CS_2 vapor is changed to (0.9, 15 s) or (0.7, 15 s). The crystallinity of P3HT is further improved for higher solvent CS_2 vapor at (0.9, 15 s), as indicated by the appearance of P3HT whiskers in TEM image (Fig. S4d†). However, the performance of corresponding device is still low; especially the J_{sc} of 8.51 mA cm^{-2} is much lower than that of the other devices prepared also upon two-step C-SVA treatment. This result hints that the efficiency enhancement *via* two-step C-SVA is not only attributed to the increased crystallinity of P3HT but also the formation of PCBM clusters with appropriate size and distribution. Higher (*e.g.* 0.9), or lower CS_2 (0.7) vapor pressure employed in the treatment will dissolve the initial PCBM aggregates more or less than actual required, resulting in smaller or larger PCBM clusters (Fig. S4c†). In contrast, an appropriate CS_2 vapor pressure at (0.8, 15 s) leads to an optimized size of around 20 nm, which contributes to the most efficient PV device obtained in the this work. Therefore, for the P3HT/PCBM device, as evidenced by the morphology optimization *via* this two-step C-SVA approach, both the improved crystallinity of P3HT and precisely controlled size of PCBM aggregates in the photoactive layer play crucial role in determining device performance. However, less attention has so far been paid to the later aspect compared to the former.

As revealed by TEM, AFM images, UV-Vis absorption and WXRD profiles described above, the morphology evolution of P3HT/PCBM composite film upon this two-step C-SVA could be schematically represented in Fig. 6. The P3HT/PCBM composite film prepared from spin coating is mainly composed of morphologically indiscernible PCBM nanocrystals and low crystalline P3HT. Upon the first step, annealing in THF vapor, PCBM molecules increase in mobility and their diffusion within the polymer matrix is not affected because of the still-low crystallinity of P3HT in the composite film. Consequently, aggregates with bigger sizes than actually required for optimized morphology are obtained. These PCBM clusters, however, will be partially dissolved by the second-step treatment in CS_2 vapor, which is mainly designed for improving the crystallinity of P3HT in the composite film. As a result, the optimized morphology with both appropriate phase size of PCBM and substantially increased crystallinity of P3HT is achieved in the photoactive layer upon this two-step C-SVA treatment, as well as improved device performance. Since in the single-step CS_2 treatment, the crystallinity of P3HT in the composite film is greatly increased upon CS_2 vapor treatment, which will substantially suppress the diffusion of PCBM within the film to form aggregates. It is crucial to keep the sequence for using THF and CS_2 for the first- and second-step vapor annealing, respectively. Otherwise, no appropriate PCBM clusters could be constructed in the composite film even upon a two-step solver vapor annealing.

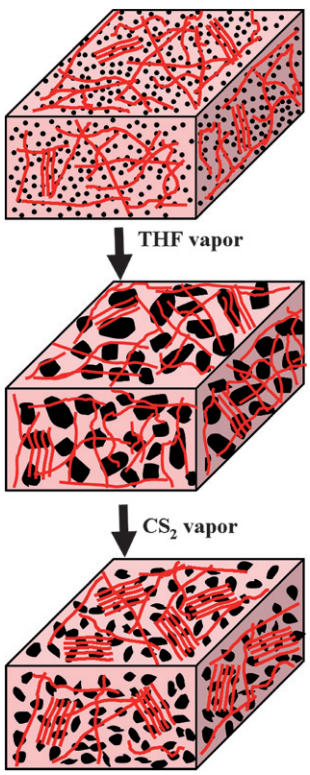

Fig. 6 Schematic illustrations of the detailed morphology evolution of P3HT/PCBM composite film upon the two-step C-SVA.

Conclusion

We have applied C-SVA to manipulate the morphology and crystallinity of a P3HT/PCBM composite film. In the single-step C-SVA, the given solvent vapor could only improve the morphology of one individual component of the composite film. Consequently, we proposed a two-step C-SVA method to tune P3HT/PCBM composite film towards so far the most precisely optimized morphology. In this new approach, THF vapor is first employed to form PCBM clusters, CS_2 vapor is afterwards used on one hand to substantially increase the crystallinity of P3HT and on the other hand to partially dissolve those large PCBM clusters, resulting in an intensively optimized morphology with both an appropriate size of PCBM aggregates and improved P3HT crystallization. The method of two-step C-SVA *via* precise control the of PCBM aggregation effectively enhances the performance. Compared with 3.2% for the thermal annealing device, PCE of two-step C-SVA device increases from 1.6% for the pristine device to 3.9%, clearly demonstrating the crucial role of morphology, in particular the precisely controlled PCBM aggregates in the composite film, on the performance of P3HT/PCBM devices.

Acknowledgements

This work was financially supported by National Natural Science Foundation of China (Grant No. 20874100, 20925415, 20990233). X.N.Y. would like to thank the Fund for Creative Research Groups (Grant No. 50621302) for financial support.

References

1 C. J. Brabec, J. A. Hauch, P. Schilinsky and C. Waldauf, *Mater. Res. Soc. Bull.*, 2005, **30**, 50.
2 F. C. Krebs, M. Jorgensen, K. Norrman, O. Hagemann, J. Alstrup, T. D. Nielsen, J. Fyenbo, K. Larsen and J. Kristensen, *Sol. Energy Mater. Sol. Cells*, 2009, **93**, 422.
3 F. C. Krebs, S. A. Gevorgyan and J. Alstrup, *J. Mater. Chem.*, 2009, **19**, 5442–5451.
4 F. C. Krebs, *Org. Electron.*, 2009, **10**, 761.
5 J. Y. Kim, K. Lee, N. E. Coates, D. Moses, T. Q. Nguyen, M. Dante and A. J. Heeger, *Science*, 2007, **317**, 222.
6 M. D. Irwin, B. Buchholz, A. W. Hains, R. P. H. Chang and T. J. Marks, *Proc. Natl. Acad. Sci. U. S. A.*, 2008, **105**, 2783.
7 Y. Y. Liang, D. Q. Feng, Y. Wu, S. T. Tsai, G. Li, C. Ray and L. P. Yu, *J. Am. Chem. Soc.*, 2009, **131**, 7792.
8 X. Yang and J. Loos, *Macromolecules*, 2007, **40**, 1353.
9 S. H. Park, A. Roy, S. Beaupre, S. Cho, N. Coates, J. S. Moon, D. Moses, M. Leclerc, K. Lee and A. J. Heeger, *Nat. Photonics*, 2009, **3**, 297.
10 Y. Kim, S. Cook, S. M. Tuladhar, S. A. Choulis, J. Nelson, J. R. Durrant, D. D. C. Bradley, M. Giles, I. McCulloch, C. S. Ha and M. Ree, *Nat. Mater.*, 2006, **5**, 197.
11 H. Hoppe and N. S. Sariciftci, *J. Mater. Chem.*, 2006, **16**, 45.
12 N. S. Sariciftci, L. Smilowitz, A. J. Heeger and F. Wudl, *Science*, 1992, **258**, 1474.
13 P. W. M. Blom, V. D. Mihailetchi, L. J. A. Koster and D. E. Markov, *Adv. Mater.*, 2007, **19**, 1551.
14 C. Yin, T. Kietzke, D. Neher and H. H. Horhold, *Appl. Phys. Lett.*, 2007, **90**, 3.
15 A. Cravino and N. S. Sariciftci, *J. Mater. Chem.*, 2002, **12**, 1931.
16 G. Yu, J. Gao, J. C. Hummelen, F. Wudl and A. J. Heeger, *Science*, 1995, **270**, 1789.
17 H. Hoppe, T. Glatzel, M. Niggemann, W. Schwinger, F. Schaeffler, A. Hinsch, M. C. Lux-Steiner and N. S. Sariciftci, *Thin Solid Films*, 2006, **511–512**, 587.
18 A. R. Campbell, J. M. Hodgkiss, S. Westenhoff, I. A. Howard, R. A. Marsh, C. R. McNeill, R. H. Friend and N. C. Greenham, *Nano Lett.*, 2008, **8**, 3942.
19 F. Yang, K. Sun and S. R. Forrest, *Adv. Mater.*, 2007, **19**, 4166.
20 M. T. Rispens, A. Meetsma, R. Rittberger, C. J. Brabec, N. S. Sariciftci and J. C. Hummelen, *Chem. Commun.*, 2003, 2116.
21 S. E. Shaheen, C. J. Brabec, N. S. Sariciftci, F. Padinger, T. Fromherz and J. C. Hummelen, *Appl. Phys. Lett.*, 2001, **78**, 841.
22 G. Li, V. Shrotriya, J. S. Huang, Y. Yao, T. Moriarty, K. Emery and Y. Yang, *Nat. Mater.*, 2005, **4**, 864.
23 L. G. Li, G. H. Lu and X. N. Yang, *J. Mater. Chem.*, 2008, **18**, 1984.
24 Y. Yao, J. H. Hou, Z. Xu, G. Li and Y. Yang, *Adv. Funct. Mater.*, 2008, **18**, 1783.
25 J. K. Lee, W. L. Ma, C. J. Brabec, J. Yuen, J. S. Moon, J. Y. Kim, K. Lee, G. C. Bazan and A. J. Heeger, *J. Am. Chem. Soc.*, 2008, **130**, 3619.
26 W. L. Wang, H. B. Wu, C. Y. Yang, C. Luo, Y. Zhang, J. W. Chen and Y. Cao, *Appl. Phys. Lett.*, 2007, **90**, 3.
27 F. Padinger, R. S. Rittberger and N. S. Sariciftci, *Adv. Funct. Mater.*, 2003, **13**, 85.
28 X. N. Yang, J. Loos, S. C. Veenstra, W. J. H. Verhees, M. M. Wienk, J. M. Kroon, M. A. J. Michels and R. A. J. Janssen, *Nano Lett.*, 2005, **5**, 579.
29 W. L. Ma, C. Y. Yang, X. Gong, K. Lee and A. J. Heeger, *Adv. Funct. Mater.*, 2005, **15**, 1617.
30 G. H. Lu, L. G. Li and X. N. Yang, *Small*, 2008, **4**, 601.
31 G. Li, Y. Yao, H. Yang, V. Shrotriya, G. Yang and Y. Yang, *Adv. Funct. Mater.*, 2007, **17**, 1636.
32 C. H. Woo, B. C. Thompson, B. J. Kim, M. F. Toney and M. J. Frechet, *J. Am. Chem. Soc.*, 2008, **130**, 16324.
33 K. A. Cavicchi and T. P. Russell, *Macromolecules*, 2007, **40**, 1181.
34 G. H. Lu, L. G. Li and X. N. Yang, *Macromolecules*, 2008, **41**, 2062.
35 Y. Lin, A. Boker, J. B. He, K. Sill, H. Q. Xiang, C. Abetz, X. F. Li, J. Wang, T. Emrick, S. Long, Q. Wang, A. Balazs and T. P. Russell, *Nature*, 2005, **434**, 55.
36 P. A. Troshin, H. Hoppe, J. Renz, M. Egginger, J. Y. Mayorova, A. E. Goryochev, A. S. Peregudov, R. N. Lyubovskaya, G. Gobsch, N. S. Sariciftci and V. F. Razumov, *Adv. Funct. Mater.*, 2009, **19**, 779.
37 C. Y. Zhang, X. J. Zhang, X. H. Zhang, X. Fan, J. S. Jie, J. C. Chang, C. S. Lee, W. J. Zhang and S. T. Lee, *Adv. Mater.*, 2008, **20**, 1716.
38 K. C. Dickey, J. E. Anthony and Y. L. Loo, *Adv. Mater.*, 2006, **18**, 1721.
39 J. C. Conboy, E. J. C. Olson, D. M. Adams, J. Kerimo, A. Zaban, B. A. Gregg and P. F. Barbara, *J. Phys. Chem. B*, 1998, **102**, 4516.
40 S. Miller, G. Fanchini, Y. Y. Lin, C. Li, C. W. Chen, W. F. Su and M. Chhowalla, *J. Mater. Chem.*, 2008, **18**, 306.
41 P. J. Brown, D. S. Thomas, A. Kohler, J. S. Wilson, J. S. Kim, C. M. Ramsdale, H. Sirringhaus and R. H. Friend, *Phys. Rev. B: Condens. Matter Mater. Phys.*, 2003, **67**, 16.
42 X. N. Yang, J. K. J. van Duren, R. A. J. Janssen, M. A. J. Michels and J. Loos, *Macromolecules*, 2004, **37**, 2151.
43 D. B. Xiao, X. Lu, W. S. Yang, H. B. Fu, Z. G. Shuai, Y. Fang and J. N. Yao, *J. Am. Chem. Soc.*, 2003, **125**, 6740.
44 T. Erb, U. Zhokhavets, G. Gobsch, S. Raleva, B. Stuhn, P. Schilinsky, C. Waldauf and C. J. Brabec, *Adv. Funct. Mater.*, 2005, **15**, 1193.

